Biochimica et Biophysica Acta 1838 (2014) 3014–3024

Contents lists available at ScienceDirect

Biochimica et Biophysica Acta

journal homepage: www.elsevier.com/locate/bbamem

The periplasmic domain of *Escherichia coli* outer membrane protein A can undergo a localized temperature dependent structural transition

Hiroaki Ishida, Alicia Garcia-Herrero, Hans J. Vogel *

Biochemistry Research Group, Department of Biological Sciences, University of Calgary, Calgary, Alberta, Canada

ARTICLE INFO

Article history:
Received 21 June 2014
Received in revised form 7 August 2014
Accepted 8 August 2014
Available online 15 August 2014

Keywords:
OmpA
Outer membrane protein A
Escherichia coli OmpA
Periplasmic peptidoglycan binding domain
TonB
Nanodisc

ABSTRACT

Gram-negative bacteria such as *Escherichia coli* are surrounded by two membranes with a thin peptidoglycan (PG)-layer located in between them in the periplasmic space. The outer membrane protein A (OmpA) is a 325-residue protein and it is the major protein component of the outer membrane of *E. coli*. Previous structure determinations have focused on the N-terminal fragment (residues 1–171) of OmpA, which forms an eight stranded transmembrane β-barrel in the outer membrane. Consequently it was suggested that OmpA is composed of two independently folded domains in which the N-terminal β-barrel traverses the outer membrane and the C-terminal domain (residues 180–325) adopts a folded structure in the periplasmic space. However, some reports have proposed that full-length OmpA can instead refold in a temperature dependent manner into a single domain forming a larger transmembrane pore. Here, we have determined the NMR solution structure of the C-terminal periplasmic domain of *E. coli* OmpA ($OmpA^{180–325}$). Our structure reveals that the C-terminal domain folds independently into a stable globular structure that is homologous to the previously reported PG-associated domain of *Neisseria meningitides* RmpM. Our results lend credence to the two domain structure model and a PG-binding function for OmpA, and we could indeed localize the PG-binding site on the protein through NMR chemical shift perturbation experiments. On the other hand, we found no evidence for binding of $OmpA^{180–325}$ with the TonB protein. In addition, we have also expressed and purified full-length OmpA ($OmpA^{1–325}$) to study the structure of the full-length protein in micelles and nanodiscs by NMR spectroscopy. In both membrane mimetic environments, the recombinant OmpA maintains its two domain structure that is connected through a flexible linker. A series of temperature-dependent HSQC experiments and relaxation dispersion NMR experiments detected structural destabilization in the bulge region of the periplasmic domain of OmpA above physiological temperatures, which may induce dimerization and play a role in triggering the previously reported larger pore formation.

1. Introduction

Escherichia coli and other Gram-negative bacteria are protected by a cell envelope that is made up of two lipid membrane bilayers and a single peptidoglycan (PG[1])-layer. A total of 2–3% of all the genes in such bacteria encode for proteins that are located in the outer membrane (OM; [1]). Outer membrane protein A (OmpA) is the major OM protein of *E. coli*. OmpA has multiple functions (reviewed in [2]) including its contribution to maintaining the outer membrane integrity [3] and F-factor dependent bacterial conjugation [4–6]. In addition, OmpA can mediate virulence and pathogenicity of *E. coli*, and it has become an important target in the immune response (reviewed in [7]). It also acts as the receptor for several bacteriophages [8–10] and colicins [11,12]. The 325-residue OmpA protein is thought to consist of two independently folded domains that are connected by a short linker [13] that can be digested by trypsin [14,15]. The N-terminal domain (residues 1–170) has been predicted to cross the OM eight times [16], and indeed it forms a narrow trans-membrane eight-stranded β-barrel structure [17,18]. Although it has been shown that OmpA forms a non-specific diffusion pore [19], the available high-resolution crystal structures do not display a continuous passage pathway for any solutes. However, molecular dynamics simulation studies have demonstrated that hydrogen bond switching inside the barrel can create a transient channel for small solutes such as water molecules and ions [20], and this mechanism has later been demonstrated experimentally [21]. Nevertheless,

* Corresponding author at: Biochemistry Research Group, Department of Biological Sciences, University of Calgary, 2500 University Drive N.W., Calgary, Alberta T2N 1N4, Canada. Tel.: +1 403 220 6006; fax: +1 403 289 9311.
E-mail address: vogel@ucalgary.ca (H.J. Vogel).

[1] The abbreviations used are: PG, peptidoglycan; NMR, nuclear magnetic resonance; HSQC, heteronuclear single quantum correlation; TCEP, Tris(2-carboxyethyl)phosphine; POPC, 1-palmitoyl-2-oleoyl-sn-glycero-3-phosphocholine; DHPC, 1,2-dihexanoyl-sn-glycero-3-phosphocholine; CPMG, Carr–Purcell–Meiboom–Gill; NOESY, nuclear Overhauser effect spectroscopy; DSS, 4,4-dimethyl-4-silapentane-1-sulfonic acid; SUMO, small ubiquitin-like modifier; CSP, chemical shift perturbation; RDC, residual dipolar coupling; DPC, dodecylphosphocholine; SDS–PAGE, sodium dodecyl sulfate–poly-acrylamide gel electrophoresis; *m*DAP, *meso*-diaminopimelic acid

http://dx.doi.org/10.1016/j.bbamem.2014.08.008
0005-2736/

this narrow channel is unlikely to allow permeation of larger molecules, given the relatively rigid backbone conformation of the barrel [22–24].

Density gradient centrifugation studies have shown that two different conformations of OmpA can be purified from the outer membrane. After separation, it was concluded that 2–3% of all OmpA proteins could form a larger pore structure [19,25]. Arora et al. have observed that incorporation of OmpA into planar lipid bilayers creates two channels with distinctive membrane conductance properties (50–80 and 260–320 pico-siemens (pS)), whereas the N-terminal truncated OmpA (residues 1–171) could only create the smaller pore [26]. This suggested that the C-terminal domain of OmpA is required for the formation of the larger pore. The structural transition from the small pore into the large pore is markedly temperature dependent [27] where the large channel becomes more prominent above physiological temperatures. On the other hand, a number of reports have indicated that the C-terminal domain of *E. coli* OmpA (residues 196–325) can form an independently folded structure with a high proportion of α-helix [16,28–30]. This portion of the protein resides in the periplasm and it may interact with the PG-layer [28,31]. Therefore, the role of the C-terminal domain of OmpA in the pore forming mechanism has remained controversial. To better understand the native conformation and the possible structural transition of *E. coli* OmpA, knowledge of the structure of its C-terminal domain, and its stability is essential. Here, we report the solution NMR structure of the isolated C-terminal domain (residues 180–325) of OmpA ($OmpA^{180–325}$) from *E. coli* strain K12. Our structure indicates that, like the N-terminal domain, the C-terminal domain can also fold independently into a stable globular structure. The structure is very similar to the previously reported bacterial PG-binding domain of *Neisseria meningitides* RmpM [32] and to other PG-associated domains such as *Haemophilus influenzae* PG-associated lipoprotein (PAL) [33]. We could also identify the PG-binding site for *E. coli* OmpA. Therefore, our results strongly support the two domain structural model of OmpA together with a PG-binding function to maintain outer membrane integrity. In order to further confirm this, we have also expressed and purified full-length OmpA ($OmpA^{1–325}$) to study the structure of the complete protein in micelles and nanodiscs by NMR spectroscopy. In particular, nanodiscs are thought to make excellent mimetics of biological membranes (reviewed in [34]). These data confirm that the full-length recombinant OmpA is also folded into two domains in these membrane mimetic environments, and that they are connected by a flexible linker. A series of temperature-dependent HSQC experiments and relaxation dispersion experiments detected structural destabilization in the bulge region of OmpA above physiological temperature, which enhances the dimerization of the protein that in turn may trigger the previously reported temperature-dependent structural alterations.

2. Materials and methods

2.1. Protein expression and purification

The full-length OmpA protein from *E. coli* strain K12 ($OmpA^{1–325}$) and its C-terminal domain ($OmpA^{180–325}$; residues 180–325; Fig. 1a) were chemically synthesized (Geneart AG) and subcloned into the pE-SUMO vector (LifeSensors, Inc., Malvern, PA) and the pET15 vector (Invitrogen), respectively, using NdeI and XhoI sites. The proteins were overexpressed in the cytoplasm of *E. coli* strain BL21 (DE3) following addition of 0.5 mM IPTG. The uniformly ^{15}N- and $^{15}N,^{13}C$-labeled $OmpA^{180–325}$ were produced from bacteria grown in minimal M9 media containing 0.5 g/L $^{15}NH_4Cl$ and 3 g/L $^{13}C_6$-glucose (or unlabeled glucose). Uniformly $^{2}H,^{15}N$-labeled $OmpA^{1–325}$ was produced from bacteria growing in M9 media containing 0.5 g/L $^{15}NH_4Cl$ in 99% $^{2}H_2O$. $OmpA^{180–325}$ was purified from the soluble fraction of the lysate using a chelating-Sepharose fast flow resin (GE Healthcare) column charged with Ni^{2+} for the immobilized metal affinity chromatography. The SUMO fusion protein was excised by SUMO proteinase I (LifesSensors, Inc., Malvern, PA). Purified $OmpA^{180–325}$ contained the cloning artifact His-Met at its N-terminus. On the other hand, full-length $OmpA^{1–325}$ was purified from inclusion bodies that were solubilized in the denaturing buffer containing 8 M urea using a Ni^{2+} column and refolded into membrane mimetic solutions as previously described [23,35]. The purified $OmpA^{1–325}$ in 8 M urea was concentrated and then diluted by adding 60 volume refolding buffer containing 15 mM DPC, 20 mM sodium borate (pH 10), 150 mM NaCl, and 1 mM EDTA followed by overnight incubation at room temperature. The refolding of the full-length protein was confirmed by SDS–PAGE as previously described ([36], Supplementary Fig. 1). The refolded protein was precipitated by addition of 0.15 volume 4 M NaCl and 20 volume cold ethanol (−20 °C). The mixture was kept at −20 °C for 4 h and then centrifuged. The pellet was washed in 1 mL of the refolding buffer and again precipitated. To produce the NMR sample of $OmpA^{1–325}$ in micelles, the pellet was resuspended in 500 mL of the NMR buffer containing 300 mM DHPC. In order to reconstitute $OmpA^{1–325}$ into the nanodiscs, the pellet was resuspended to 30 μM in the solution containing 120 μM of the MSP1D1 nanodisc protein [37], 8 mM POPC, 16 mM sodium cholate, 20 mM Tris–Cl (pH 7.5), 100 mM NaCl and 0.5 mM EDTA and incubated for 1 h at room temperature. The gene for the MSP1D1 nanodisc protein was chemically synthesized (Geneart AG) with an N-terminal His-tag and subcloned into the pET15 vector. The protein was expressed and purified analogous to the procedure described above. The detergent was removed by addition of 80% (w/v) Bio-Bead SM2 (Bio-Rad) followed by 2 h incubation at room temperature and then the beads were removed by passing through a 0.45 μm filter. The formation of uniformly sized $OmpA^{1–325}$/POPC nanodiscs was analyzed by S200 gel filtration chromatography, where the column was equilibrated with a buffer containing 20 mM sodium phosphate (pH 6.5), 50 mM NaCl and 0.5 mM EDTA (Supplementary Fig. 1). The fractions containing the $OmpA^{1–325}$/POPC nanodiscs were pooled and concentrated down using a centrifugal filter unit (Amicon) to the NMR sample.

2.2. NMR measurements

All NMR samples of $OmpA^{180–325}$ contained approximately 0.5 mM ^{15}N- or $^{15}N,^{13}C$-labeled $OmpA^{180–325}$, 20 mM sodium phosphate buffer (pH 6.0), 0.03% NaN_3, and 0.5 mM 2,2-dimethyl-2-silapentane-5-sulfonate (DSS) in 90% H_2O/10% D_2O or 99.9% D_2O. The NMR sample of $OmpA^{1–325}$ in the DHPC micelles contained approximately 0.5 mM $^{2}H,^{15}N$-labeled $OmpA^{1–325}$, 300 mM DHPC, 20 mM sodium phosphate buffer (pH 6.5), 100 mM NaCl, and 0.03% NaN_3 in 90% H_2O/10% D_2O. The NMR sample of $OmpA^{1–325}$ in the POPC nanodiscs contained approximately 0.1 mM $^{2}H,^{15}N$-labeled $OmpA^{1–325}$ embedded in the POPC/MSP1D1 nanodisc, 20 mM sodium phosphate buffer (pH 6.5), 50 mM NaCl, and 0.5 mM EDTA. Residual Dipolar Coupling (RDC) measurements were achieved using the pentaethylene glycol monododecyl ether/1-hexanol system (3%, $r = 0.96$) as previously described [38]. All NMR experiments required for the structural determination were performed at 25 °C on Bruker Avance 500 or 700 MHz NMR spectrometers equipped with triple resonance inverse Cryoprobes with a single axis z-gradient. Sequential assignments of HN, N, CO, C_α, and C_β resonances of $OmpA^{180–325}$ were achieved using a series of three-dimensional experiments including CBCANH, CBCA(CO)NH, HNCO and HN(CA)CO. Aliphatic side-chain assignments were obtained through three-dimensional C(CCO)NH-TOCSY, H(CCO)NH-TOCSY, and HBHA(CBCACO)NH experiments. Assignment of aromatic side-chains was achieved using two-dimensional (HB)CB(CGCD)HD and (HB)CB(CGCDCE)HE experiments. All NOESY experiments including three-dimensional ^{15}N-edited NOESY-HSQC and ^{13}C-edited NOESY-HSQC, and two-dimensional NOESY were measured with a mixing time of 100 ms. H–N RDC measurements were performed using the in-phase/anti-phase (IPAP)-($^{1}H,^{15}N$)-HSQC experiment. All NMR experiments for the backbone dynamics studies of the ^{15}N-labeled $OmpA^{180–325}$ were acquired at 50.68 MHz for the ^{15}N frequency. The ^{15}N T_1 data

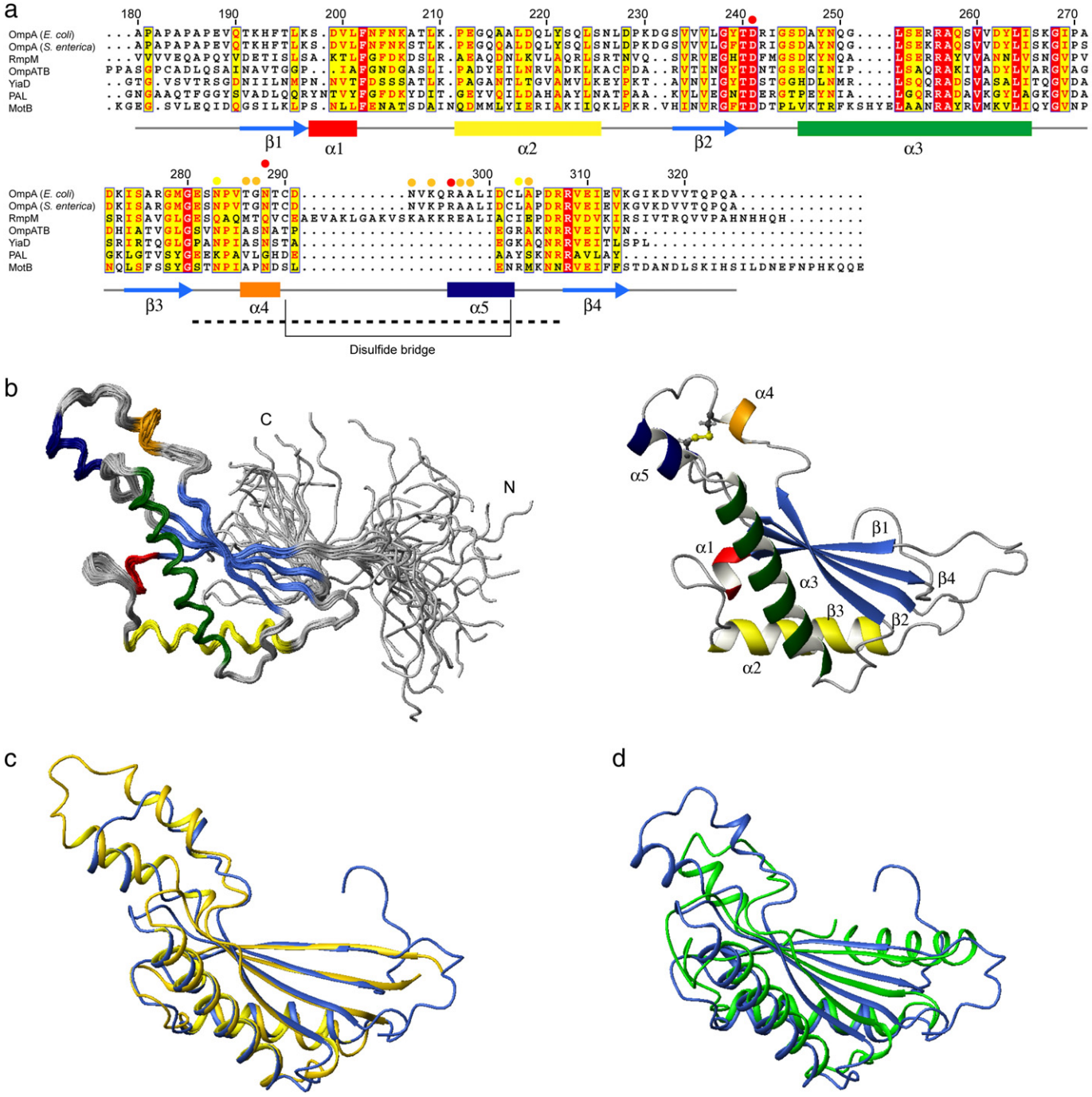

Fig. 1. a) The amino-acid sequence of the C-terminal domain of *E. coli* OmpA (180–325) is aligned with the PG-binding domains from different periplasmic proteins including *Neisseria meningitidis* RmpM, *Mycobacterium tuberculosis* OmpATB, *E. coli* YiaD, *Haemophilus influenzae* PAL, and *Helicobacter pylori* MotB. The positions of the secondary structure elements determined for OmpA are also displayed and a broken line indicates the region of the bulge structure. The residues that show an intensity loss and/or a slow motion in NMR time scale at higher temperature are indicated using the same color code as Fig. 5. b) The 30 lowest energy structures of $OmpA^{180–325}$ are superimposed using the backbone atoms of residues 191–314 (left panel). Ribbon representation of the lowest energy structure of $OmpA^{180–325}$. All the secondary structure elements are colored differently and are labeled (right panel); the disulfide bond is also displayed. c) $OmpA^{180–325}$ is compared to the PG-binding domains of RmpM (left panel; PDB ID: 1R1M) and MotB (right panel; PDB ID: 3CYP). $OmpA^{180–325}$ is colored in blue in both panels.

were acquired using ^{15}N relaxation delays of 14 (×2), 98, 350, 490 (×2), 700, 896, and 1190 ms in a randomized order with a recycle delay of 1.5 s. The ^{15}N T_2 relaxation data were obtained using a Carr–Purcell–Meiboom–Gill (CPMG)-type T_2 experiment, where the field strength of the 180° pulse was 5 kHz, and the 180° pulses were applied every 1 ms. The relaxation delays used were 8.8 (×2), 17.6, 26.4 (×2), 35.2, 44.0, 70.4, and 79.2 ms in randomized order. The recycle delay used was 2.5 s. $\{^1H\}$–^{15}N heteronuclear NOE data were obtained using a 4 s train of 120° proton pulses. The ^{15}N relaxation dispersion measurements were acquired by using standard experiments and the decay rate, R_2^{eff}, was obtained for two different rf fields of CPMG (0.05 kHz and 1 kHz) using the formula described previously [39]. The length of the CPMG period was kept constant at 40 ms for both experiments. The reference spectrum was obtained using the same experiment omitting the CPMG period. To investigate the PG-binding properties of $OmpA^{180–325}$, N-acetylglucosamine (NAG), N-acetylmuramic acid

(NAM), and PG tri-peptide: L-Ala-D-γ-Glu-mDap (Anaspec, Inc., San Jose, CA) were titrated into samples containing ^{15}N-labeled OmpA$^{180–325}$. The concentration of the PG tri-peptide was estimated from the peak volume relative to that of DSS with known concentration. Chemical shift perturbations (CSP) were monitored by recording ^{1}H,^{15}N-HSQC experiments. All spectra were processed using NMRPipe/NMRDraw [40] and analyzed using the NMRView software [41].

2.3. Structure calculation

The initial structure of OmpA$^{180–325}$ was calculated with CYANA [42] version 2.0 using distance restraints derived from the automated NOE assignment protocol implemented in CYANA, α-helix hydrogen bond restraints based on the secondary structure from the chemical shift index, and dihedral angle restraints as predicted by TALOS+ [43]. The hydrogen bond restraints for β-sheets were carefully introduced in the later stages of the calculations. The C_β signals of Cys219 and Cys302 appeared in the chemical shift range expected for oxidized Cys residues (40.1 and 40.6 ppm, respectively). The addition of a reducing agent, TCEP caused a large change in ^{1}H,^{15}N-HSQC spectra (data not shown). These data confirm that the disulfide bond was spontaneously formed during the protein preparation. Therefore, the disulfide bond between these Cys residues was also implemented in the structure calculation. Further structure refinement with the addition of backbone H–N RDC restraints were performed by XPLOR-NIH [44] version 2.20. Initial estimates for the axial component of the molecular alignment tensor (Da) and the rhombicity (R) were obtained from the lowest energy structure calculated by CYANA using PALES [45]. Finally, the 30 lowest energy structures from a total of 200 were selected and used for the analysis. All molecular graphics used in this manuscript were created using MOLMOL [46].

2.4. Rotational diffusion dynamics

The ^{15}N T_1 and T_2 data were fitted with the program CurveFit (A. G. Palmer, Columbia University). The uncertainties for the peak intensity used for the fitting were estimated from duplicated data points. The uncertainty for the {^{1}H}–^{15}N NOE values was evaluated using the standard deviation of the noise in empty spectral regions of the spectra. Those residues that show low NOE values (less than 0.65) were excluded from further analysis, because these residues have a slow internal motion which contributes to the T_1 relaxation. Those residues which are involved in chemical exchange processes that affect the T_2 relaxation time were detected and removed as described by Tjandra et al. [47]. For the remaining residues, the rotational correlation time for the global tumbling (τ_m) for each residue were estimated from the R_2/R_1 ratio using the program $R_2R_1\_t_m$ (A. G. Palmer, Columbia University). The τ_m values were globally fit to the OmpA$^{180–325}$ structure using the program quadric_diffusion (A. G. Palmer, Columbia University).

2.5. Differential scanning calorimetry

DSC experiments were performed on a VP-DSC microcalorimeter (MicroCal, GE Healthcare). The sample contained 30 μM OmpA$^{180–325}$ and 20 mM HEPES (pH 7.0). The heating scan consisted of a 15-min pre-scan thermostat period at 10 °C, and a 10–125 °C heating scan with the rate of 90 °C/h with a filter period of 16 s, and passive thermal compensation between the sample and reference cells. The subtraction of the baseline and the melting curve fitting were performed using MicroCal Origin software. The experiments were repeated several times with different sample concentrations and scanning rates and all produced very similar results.

2.6. In vitro cross-linking experiments

In vitro cross-linking experiments were performed with DPM (dimethyl pimelimidate). The samples contained 150 μM OmpA$^{180–235}$, 20 mM sodium phosphate buffer (pH 8.0), and 100 mM NaCl. Samples with and without 3 mM DPM were incubated for 1 h at 25, 37 or 42 °C. The cross-linked protein was detected by SDS–PAGE and Coomassie brilliant blue staining.

The atomic coordinates and resonance assignments have been deposited in the Protein Data Bank (PDB ID: 2MQE) and the BMRB database (BMRB-25030), respectively.

3. Results

3.1. NMR structure determination

All backbone amide resonances of the C-terminal domain of OmpA from *E. coli* (OmpA$^{180–325}$) could be assigned in the ^{1}H,^{15}N-HSQC spectrum (Fig. 2) except for a few residues including Lys206, Ala207, R242, and I243 that were not detected most likely due to severe broadening caused by chemical exchange. In addition, three Ala residues in the N-terminal Ala-Pro repeat could not be unambiguously assigned, however it was confirmed that this region of the protein was completely disordered (see below). In addition, the slightly truncated protein, OmpA$^{188–325}$, in which the Ala-Pro repeat region from the linker is omitted, produced an HSQC spectrum that is essentially identical to that of OmpA$^{180–325}$ (Supplementary Fig. 2). This result confirms that the inter-domain linker region is not important for the overall folding of this domain. The chemical shift index (CSI) analysis using Cα and C′ atoms revealed that periplasmic OmpA$^{180–325}$ domain contains several α-helices consistent with previous circular dichroism spectroscopy observations (Fig. 3; [29]). The side-chain ^{1}H resonance assignments could be obtained for 91.7% of all the ^{1}H resonances. The initial structures were calculated using torsion angle dynamics and the automated NOE assignment protocol of CYANA. 2437 NOE cross-peaks in the 3D ^{15}N- and ^{13}C-NOESY-HSQC spectra were automatically assigned by CYANA and this generated 1960 upper distance restraints. The distribution of the distance restraints available along the protein sequence is displayed in Fig. 3a. The calculated structure contained a relatively large bulge structure from residues 281 to 307 (see below), which did not show significant interactions with the rest of the OmpA$^{180–325}$ structure. Therefore, in order to position this part of the structure correctly, we have employed backbone H–N RDCs in further refinements of the structure with the program XPLOR-NIH. The RDC values were

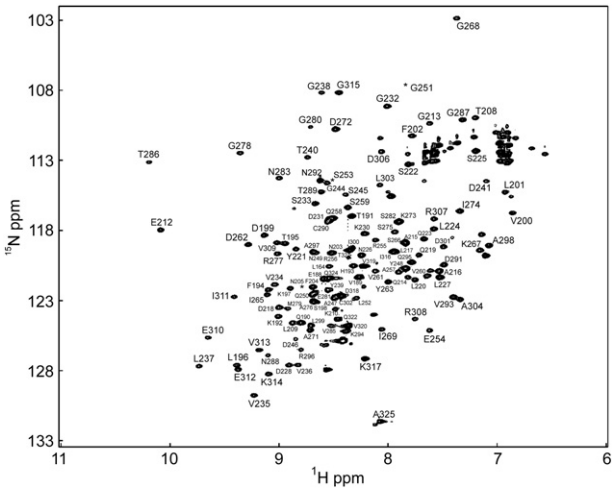

Fig. 2. The assigned ^{1}H,^{15}N HSQC spectrum of OmpA$^{180–324}$. The positions of the signals that are invisible at this contour level are indicated with asterisks. The spectrum was acquired at 25 °C.

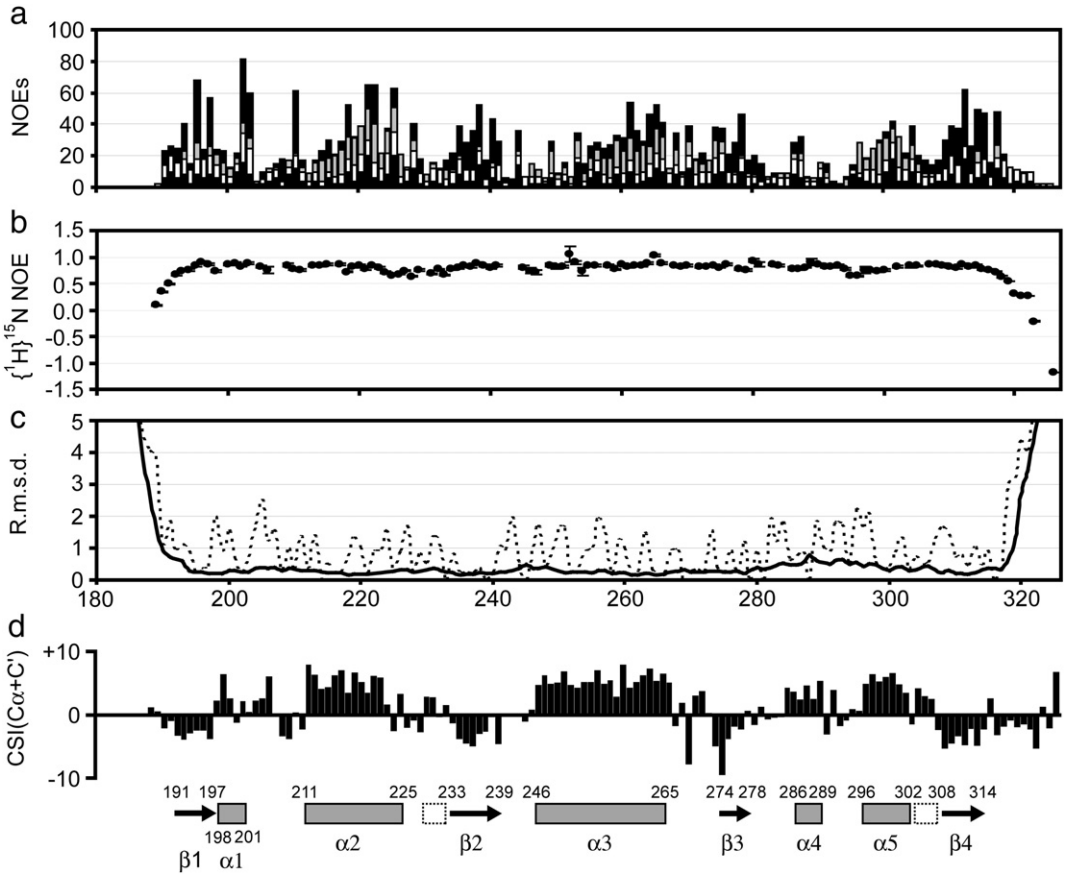

Fig. 3. Structural data for OmpA$^{180–325}$. a) The number of distance restraints for the structure calculation. White, gray, dark gray, and black bars indicate the number of intra-residue, sequential, medium range (2–4), and long range (5+) NOEs, respectively. b) The backbone {^{1}H},^{15}N-NOE. c) The r.m.s.d.'s of the 30 calculated structures for the backbone and all the heavy atoms are plotted with a solid and dashed line, respectively. d) CSI values for C_α and C′ atoms. The secondary structures obtained from the calculated structures are also shown. The boxes and arrows with residue numbers indicate the position of the helices and sheets, respectively. Two irregular helices are also indicated by the boxes with a broken line.

successfully measured for 99 residues ranging between -20.7 and 29.4 Hz. The backbone r.m.s.d. for the well-folded region (residues 192–314) of the calculated 30 structures with the lowest energy was 0.38 ± 0.08 Å (Fig. 1b). There are no considerably flexible regions except for the N- and C-terminal ends of the protein in agreement with the {^{1}H},^{15}N hetero-nuclear NOE data (Fig. 3b and c). A total of 99.6% of the residues were found in the favored region or the additionally allowed regions of the PROCHECK Ramachandran plot and no residues were found in the disallowed regions. All the structural parameters from the final stage of the structure calculation are summarized in Supplemental Table 1. The main architecture of OmpA$^{180–325}$ consists of two long α-helices and four β-strands which form a combination of parallel and anti-parallel β-sheets, which is referred to as "βαβαββ" fold (Fig. 1b; [48]). The OmpA$^{180–325}$ structure also features a relatively large bulge containing two small α-helices bridged by a disulfide bond between Cys219 and Cys302 that is relatively isolated from the main structure. The positions of all the secondary elements are consistent with those predicted from the chemical shifts (Fig. 3d).

3.2. Structural comparisons of OmpA$^{180–325}$ with other OmpA-like domains

Recently, the crystal structure of the C-terminal domain of *Salmonela enterica* OmpA has been deposited (without a detailed publication) in the Protein Data Bank (PDB ID: 4ERH). The structure appears to be a dimer containing two slightly different conformations (the backbone r.m.s.d. to each other is 2.0 Å). Surprisingly, despite the fact that this domain shares >94% sequence identity to OmpA$^{180–325}$, our structure is different in some regions, resulting in a backbone r.m.s.d. of 2.7 Å and 2.0 Å to chains A and B, respectively (discussed below). The small differences may be due to crystal packing restraints. Other than *S. enterica* OmpA, the results from a search in the database for homologous structures using the program DALI [49] found that the structurally closest homolog was RmpM [32], a peptidoglycan-binding protein from the Gram-negative bacteria *Neisseria meningitidis*. The amino acid sequence identity compared to RmpM is 35.8% and the backbone r.m.s.d. is 2.48 Å (Fig. 1a and c). The main structure (βαβαββ fold) is almost identical however the bulge region is different. *N. meningitidis* RmpM has an even larger bulge that includes two longer α-helices, but they are linked in a similar manner by a disulfide bridge. Other known bacterial peptidoglycan-binding domain protein structures include the flagellar motor protein, MotB from *Helicobacter pylori* (Fig. 1a and c; [50]), the peptidoglycan-associated lipoprotein, PAL from *H. influenzae* [33] and YiaD from *E. coli* [51], and the outermembrane protein A from *Mycobacterium tuberculosis* (OmpATB; [52]) and these were also found to be structurally closely related. The sequence identity/the best-fit backbone r.m.s.d. of OmpA$^{180–325}$ to these proteins are MotB: 18.06%/7.53 Å, YiaD: 27.4%/6.66 Å, OmpATB: 28.57%/5.93 Å, and PAL: 22.45%/8.07 Å. Regardless of the low sequence identity the main structure is very similar in all cases although the last β-strand of *E. coli* OmpA is replaced with an α-helix in several of these proteins. The remarkable difference compared to OmpA is again the bulge structure and all these proteins have a much smaller bulge region containing a single small α-helix and no disulfide bond, in contrast to OmpA and RmpM.

3.3. ^{15}N-dynamics studies by NMR spectroscopy

It has been shown through in-cell cross-linking studies and proteomics analysis that the C-terminal domain of OmpA can form a dimer

in vivo [53]. Most recently, studies using a combination of mutagenesis and mass spectrometry have confirmed the presence of such a dimeric form in vitro [54]. Indeed, the C-terminal domain of the homologous *S. enterica* OmpA protein appears as a dimer in the asymmetric unit (PDB ID: 4ERH). Moreover, the periplasmic domain of RmpM has also been shown to form a dimer in vitro [32]. Therefore, we have examined whether *E. coli* OmpA$^{180–325}$ also forms a dimer in our solution conditions using NMR techniques. NMR dynamics experiments that measure the T_1 and T_2 relaxation times of the backbone ^{15}N atoms have been performed (Supplementary Fig. 3). Reliable ^{15}N relaxation data were available for 130 residues of OmpA$^{180–325}$. After filtration of the relaxation data (see Materials and methods section), 93 residues were selected for analyzing the rotational diffusion properties of OmpA$^{180–325}$ in solution. The correlation time (τ_m) for each residue

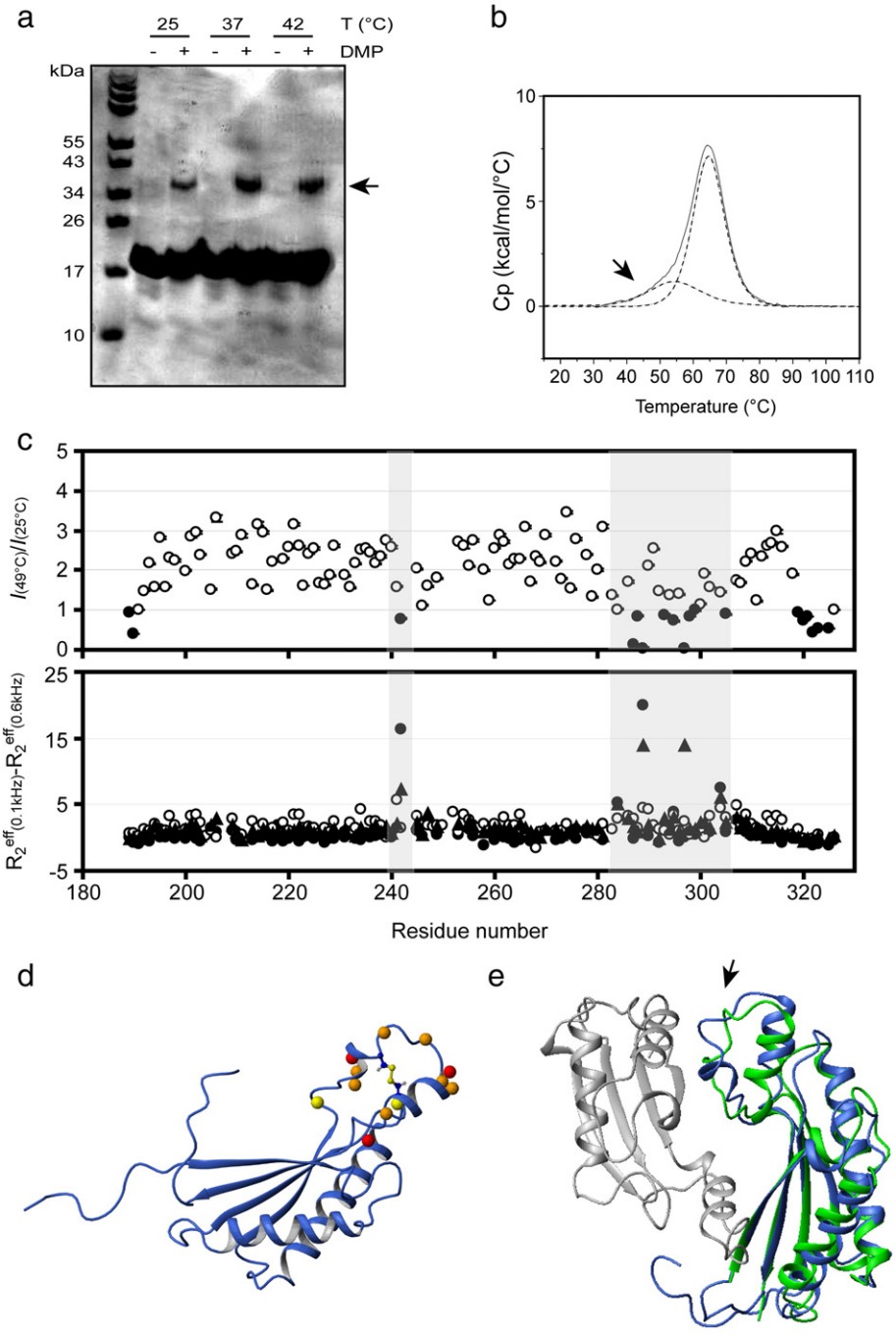

Fig. 4. a) Cross-linked proteins could be detected by SDS–PAGE. The protein bands originating from dimeric OmpA$^{180–235}$ are indicated with an arrow. b) The thermal denaturation of OmpA$^{180–325}$ was monitored by DSC. The temperature dependence of the excess heat capacity (solid line) was fitted to two different structural transitions (dotted lines). The small heat detected before the main denaturation is indicated by an arrow. c) The intensity ratios of the signals in ^{1}H,^{15}N-HSQC spectra recorded at 25 and 49 °C are plotted as a function of the residue number (top). The open and filled circles represent an intensity gain and loss, respectively. The differences between R_2^{eff} values with different CPMG frequencies (0.05 kHz and 1 kHz) are plotted for each residue (bottom). The data obtained at 25, 37, and 42 °C are plotted with open circle, triangle, and filled circle, respectively. The shaded area experiences the structure destabilization above physiological temperature. d) The residues with intensity loss in the shaded regions are mapped in orange on OmpA$^{180–325}$. The residues that show significant slow motion are shown in yellow. The residues that experience both are shown in red. e) The structure of OmpA$^{180–235}$ is superimposed onto the crystal structure of *Salmonella enterica* OmpA (PDB ID: 4ERH) using chain B. Chain A is also shown in gray. The bulge region that displays temperature dependent structural differences seems to provide an interface for dimerization in the *S. enterica* structure (pointed by the arrow).

was estimated from the R_2/R_1 ratio and ranged between 9.3 and 15.4 ns (Supplementary Fig. 3). The τ_m data was globally fitted to the OmpA$^{180–325}$ structure using the axially symmetric diffusion model. Finally, the correlation time for the overall molecular tumbling of OmpA$^{180–235}$ was defined to be 12.8 ns. This value is somewhat larger than what is expected for a monomer but it is much smaller than expected for a dimeric protein, suggesting that a monomeric-dimer equilibrium may exist in solution. The parameters obtained from this analysis are summarized in Supplemental Table 2.

3.4. In vitro chemical cross-linking experiments

The results from the rotational diffusion NMR were further evaluated by in vitro cross-linking experiments (Fig. 4a). Although a very weak band could be observed at a position on the SDS gel corresponding to the dimeric OmpA$^{180–325}$, the majority of the proteins (>90%) appear as a monomeric protein when the samples were incubated at 25 °C. Therefore, we have concluded that although a very small population of dimeric protein may exist, OmpA$^{180–325}$ is essentially monomeric in solution under our experimental conditions. This is in agreement with the recent report that the C-terminal domain of OmpA exists as a mixture of monomers and a smaller amount of dimer [54]. We have also noticed that when the incubation temperature was increased to 37 °C, the amount of the dimeric OmpA$^{180–325}$ increased by about 50% (Fig. 4a). However, further increasing the temperature to 42 °C did not cause any additional changes.

3.5. Structure destabilization by increasing the temperature

The thermal denaturation of OmpA$^{180–325}$ was monitored by DSC and its melting curve could be fit to the sum of two distinctive melting temperatures (T_ms) (Fig. 4b). The main denaturation occured at 64.8 °C with the enthalpy of denaturation (ΔH_d) of 2.49×10^4, however a smaller amount of heat was also released at 54.7 °C. Therefore, we have attempted to determine which part of OmpA$^{180–325}$ undergoes unfolding prior to the main denaturation event. ^{1}H,^{15}N-HSQC spectra were acquired at 3 °C intervals between 25 and 49 °C (Supplementary Fig. 4a) and the intensity changes were monitored for each residue. Although the majority of the signals gained in intensity by raising the temperature (because of the accelerated molecular tumbling leading to slower relaxation), several signals lost intensity around physiological temperature (Supplementary Fig. 4). Intensity ratios at 25 and 49 °C were plotted as a function of the residue number in Fig. 4c. Whereas some intensity losses were observed for the residues from both termini of OmpA$^{180–325}$, those regions are disordered and fully exposed to the solvent (Fig. 1b and Fig. 3). Therefore, an enhanced exchange rate of the amide HN group is most likely responsible for these intensity losses. However, the region in the middle of the OmpA$^{180–325}$ structure also exhibited many residues with a loss of intensity.

To obtain more information about possible motions in the protein, we have also performed NMR relaxation dispersion experiments to monitor slow motions (from micro- to millisecond). A structural exchange process could be detected for several residues only when the temperature was increased above 37 °C and these residues are identical to the ones experiencing a loss of intensity by raising the temperature (shaded area in Fig. 4c). These results corroborate the notion that these residues undergo slow conformational exchange on the NMR timescale. When these residues are highlighted on the OmpA$^{180–325}$ structure (Fig. 4d), taken together with the outcome of the DSC experiments, it seems reasonable to conclude that the bulge region of OmpA$^{180–325}$ (residues 283–304) becomes unstable above physiological temperature and denatures at an approximately 10 °C lower temperature than the main structure.

3.6. The peptidoglycan (PG) binding site of OmpA$^{180–325}$

The ability of the C-terminal domain of OmpA to interact with PG was examined using three components of the *E. coli* PG-unit, N-acetyl muramic acid (NAM), N-acetylglucosamine (NAG) and PG-tri-peptide (L-Ala-D-γ-Glu-mDap) which were titrated into ^{15}N-labeled OmpA$^{180–325}$. Chemical shift perturbations (CSPs) were monitored by recording ^{1}H,^{15}N-HSQC spectra at 25 and 42 °C. The results were very similar at both temperatures. The addition of the PG-peptide caused obvious CSPs in fast to intermediate exchange on the NMR timescale (Fig. 5a and b). However, NAM and NAG caused neither chemical shift changes nor signal broadening, suggesting no interaction. The loss of intensity was plotted for each residue (Fig. 5a) and the residues that exhibited a significant intensity loss were highlighted on the OmpA$^{180–325}$ structure (Fig. 5c). The structure was then superimposed onto the structure of *Acinetobacter baumannii* OmpA (AbOmpA) that is complexed with a PG-peptide [55]. It is clear that binding of the PG-peptide to *E. coli* OmpA180-325 causes a series of CSPs that includes the conserved D241 residue (D271 in AbOmpA) that is thought to directly interact with the *m*DAP residue of the peptide. Another important residue R258 (R286 in AbOmpA) could not be directly analyzed due to signal overlap however the adjacent residue A257 was influenced by the binding. These results indicate that OmpA$^{180–325}$ binds to the *m*DAP residue of the penta-peptide of the *E. coli* PG-layer probably in a similar fashion as AbOmpA.

3.7. A TonB binding site on OmpA$^{180–325}$?

The TonB protein is intimately involved in energy transduction across the periplasmic space [56,57]. This protein is known to span the entire periplasmic space with its N-terminus anchored in the inner membrane, while its folded C-terminal domain can be cross-linked in vivo to the outer membrane [58]. The exact location of the TonB binding site on the outer membrane is currently unknown, although some studies have suggested that the Lpp and OmpA proteins may play a role in this process [59]. Binding to the periplasmic domain of OmpA would position the TonB protein at the correct location in the periplasm to grab on to the so-called TonB-box regions from the relevant outer membrane receptors [60]. We therefore studied the binding of the unlabeled TonB domain (residues 103–239) [61] to the isotope-labeled ^{15}N-OmpA$^{180–325}$ domain. In addition, we also recorded HSQC NMR spectra to follow the binding of unlabeled OmpA$^{180–320}$ to ^{15}N isotope-labeled TonB$^{103–239}$. No chemical shift differences were detected in the NMR spectra, we therefore conclude that these two domains are unable to bind each other in vivo, unless additional components are involved that can stabilize or mediate this interaction.

3.8. Structural insights into full-length OmpA$^{1–325}$ in membrane mimetic environments

In order to determine if there are any interactions between the two independently folded regions of OmpA, we also studied the intact protein in membrane mimetic environments. The ^{1}H,^{15}N-TROSY spectra obtained for full-length OmpA$^{1–325}$ in DHPC micelles and in POPC/MSD1 nanodiscs are compared with that of OmpA$^{180–325}$ (Fig. 6). OmpA$^{1–325}$ in the DHPC micelles produced a high quality spectrum, where peaks for both the N-terminal and C-terminal domain could be seen. On the other hand, we had some difficulty to concentrate OmpA$^{1–325}$ in the nanodiscs. With the low sample concentration, the signals from the N-domain which is directly embedded in the nanodiscs are not visible due to the large overall molecular size, while almost all the signals from the C-domain are visible, suggesting that the two domains are connected by a flexible linker and that they experience very different correlation times. All the signals from the C-domain of OmpA$^{1–325}$ appear in very similar region of the spectra as those of

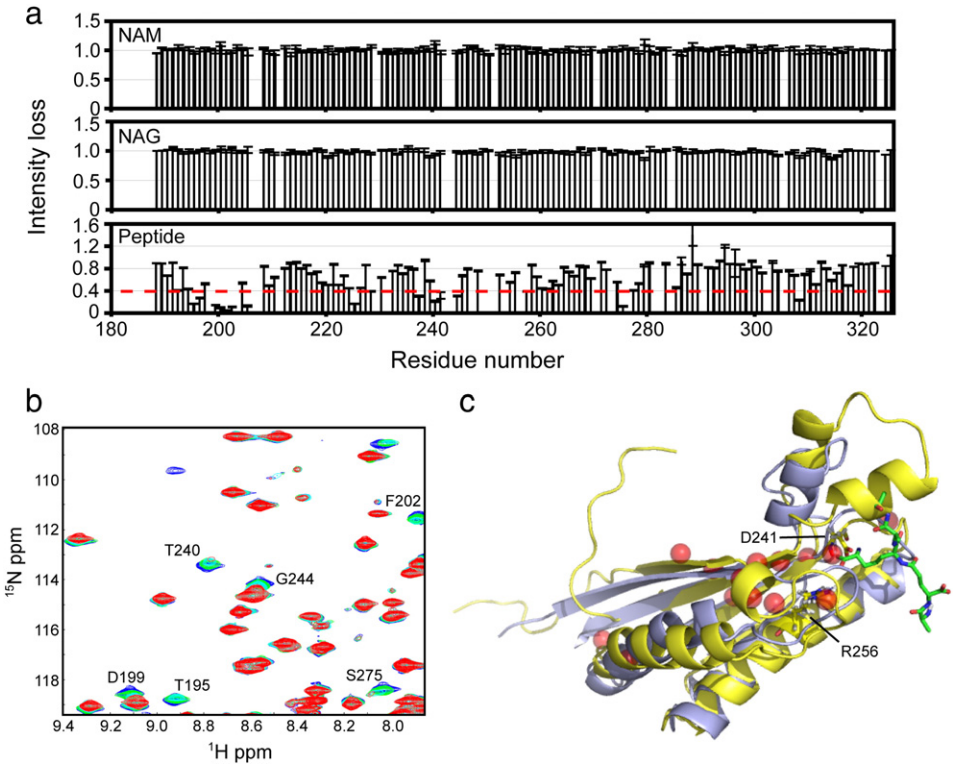

Fig. 5. a) The intensity losses in the $^{1}H,^{15}N$-HSQC spectra of OmpA$^{180–325}$ observed after addition of NAM (top), NAG (middle), and PG-tri-peptide (bottom) are plotted as a function of the residue number. b) The selected region of the overlaid $^{1}H,^{15}N$-HSQC spectra of OmpA$^{180–325}$ with different amount of PG-peptide. The residues that are influenced are labeled. c) The residues with a significant intensity loss (<0.4) are highlighted on the OmpA$^{180–325}$ structure as red spheres. OmpA$^{180–325}$ in yellow is then superimposed on to the PG-binding domain of AbOmpA in the complex with a PG-peptide shown in purple (PDB ID: 3TD5). The bound PG-precursor is displayed as a green stick. The side chains of D241 and R256 of OmpA$^{180–325}$ which may directly interact with the DAP residue of PG-peptide are also shown.

OmpA$^{180–325}$. We conclude that the C-domain structure is located outside of the membrane and retains the same structure as that of the OmpA$^{180–325}$ in both membrane mimetic environments.

4. Discussion

In this work we have determined the solution structure for the carboxy-terminal periplasmic domain of the *E. coli* OmpA protein. This part of the protein adopts a characteristic fold that is seen in many other bacterial periplasmic peptidoglycan-binding proteins. Through NMR chemical shift perturbation experiments we could determine the binding site for peptidoglycan (see Fig. 5). These results indicated that the unique diaminopimelic acid of Gram-negative PG plays a major role in the recognition, similar to what has been reported for *A. baumannii* OmpA [55]. The individual sugar moieties of PG, NAM and NAG did not appear to bind to the periplasmic domain of OmpA. This raises questions about previous modeling and docking studies for those carbohydrates when binding to the related RmpM protein [32]. We also noted that previous suggestions that the TonB protein would bind to OmpA [59] were not supported by our experimental results. An interesting feature of the *E. coli* OmpA periplasmic domain structure is the bulge region which seems to be grafted onto the protein sequence and is stabilized by a disulfide bond. Interestingly, the only other two related proteins which are known to have a similar bulge region (RmpM and *S. enterica* OmpA) also have a disulfide bond located in exactly the same position showing that these two features seemingly evolved together. The majority of the OmpA related proteins that have been structurally characterized to date do not have a bulge or the disulfide linkage.

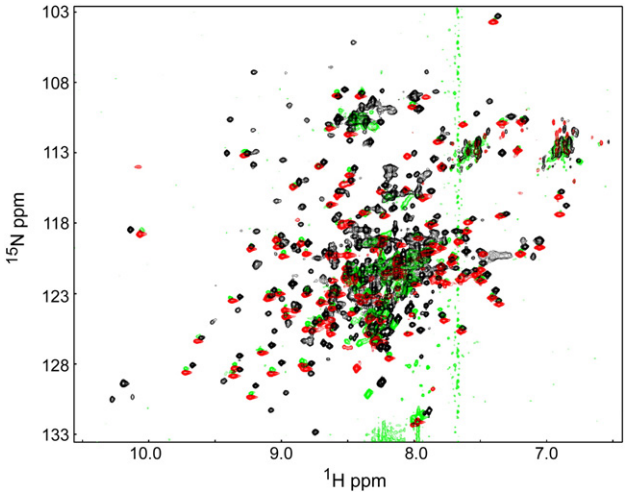

Fig. 6. Superposed $^{1}H,^{15}N$-TROSY spectra of ^{15}N-labeled OmpA$^{180–325}$ (red) in aqueous solution, $^{2}H,^{15}N$-labeled OmpA$^{1–325}$ in the DHPC micelles (black) and the POPC/MSP1D1 nanodiscs (green). All spectra were acquired at 42 °C.

The C-terminal domain of *E. coli* OmpA has previously been proposed to act as a PG-binding domain because of the high sequence similarity and the presence of several conserved residues compared to other known PG-associated domains. For example, the C-terminal domain of *Pseudomonas aeruginosa* OprF which shares 39% amino-acid sequence identity to its counterpart in *E. coli* OmpA also interacts with PG [31,28,62]. Our data showed that the penta-peptide portion of *E. coli* PG-layer could interact with the C-terminal domain of *E. coli* OmpA. The chemical shift perturbations caused by the addition of the PG-peptide appeared to be in fast to intermediate exchange on the NMR timescale (Fig. 5b), suggesting a relatively weak interaction. This is consistent with the recent report that the K_d of the PG-peptide binding to the PG-binding domain of *A. baumannii* OmpA is 10^{-6} M [55]. This

relatively weak interaction may explain why we did not observe any co-purified PG-precursor together with *E. coli* OmpA$^{180–325}$. This differs from a previous report concerning the related *H. influenzae* PAL protein [33], where a ^{13}C signal in the 100 ppm region corresponding to the C1 atom of the disaccharide of the PG-precursor was detected in the $^{1}H–^{13}C$ HSQC spectrum; this signal is lacking in the spectrum of *E. coli* OmpA (data not shown). These data suggest that PAL, which is also anchored to the outer membrane, albeit through attached fatty acids, has a higher affinity for PG than OmpA.

The permeability of the bacterial membrane is governed by a set of integral porins that are located in the OM. Together, these proteins are the major determinants of the susceptibility of bacteria to numerous antibiotics (reviewed in [63,64]). For example, *P. aeruginosa* has intrinsic resistance to many antibiotics due to the low permeability of its OM (one hundred times lower permeability than *E. coli*; [65]). One of the major porins of *P. aeruginosa*, OprF is closely related to *E. coli* OmpA in its amino-acid sequence and functional aspects, and a large population of it exists as a closed pore, which is thought to be responsible for the resistance. Given that OmpA is one of the most abundant *E. coli* porins (100,000 copies/cell; [66]), it is important to gain a better understanding of its pore forming mechanism. Recently, the idea that the *E. coli* OmpA protein can give rise to two distinctive porin conformations has received strong experimental support (reviewed in [67]). The larger pore is only observed when the C-terminal domain of OmpA is present and the population of it drastically increased above physiological temperature ([26,27]). The absence of OmpA in *E. coli* causes deficiency in the uptake of amino acids such as glutamine and proline, and this effect is more apparent when the temperature was increased from 30 °C to 42 °C [68]. Furthermore, it has been shown that only a very small percentage of OmpA proteins were able to form a large pore when the experiments were carried out at low temperature [19]. Taken together, these data suggest that the population of OmpA capable of forming a large pore depends on the temperature. However, the structure of the C-terminal domain of OmpA, OmpA$^{180–325}$, represents a well folded globular conformation with no obvious flexible or unstable regions except for both termini at 25 °C (Fig. 3) and it is highly soluble and stable in solution. Thus, it seems unlikely that this would completely unfold and then insert itself into the outer membrane to help create a large pore. Our NMR data obtained for the full-length OmpA protein in two membrane mimetic environments are also consistent with the notion that OmpA is comprised of two separate domains even at 42 °C (Fig. 6), although we cannot rule out the possibilities that a small amount of alternatively folded protein is not visible in our NMR spectra.

In this contribution, we have carefully examined the thermal stability of the C-domain in an attempt to discover any signs of a structural transition around the physiological temperature. Our data showed that the characteristic bulge region (residues 288–304) of OmpA$^{180–325}$ is more sensitive to heat than the rest of the structure and that it becomes unstable above physiological temperatures (Fig. 4). The bulge structure is made up of two small helices and a single disulfide bridge. Since this region is found in only a subset of bacterial OmpA proteins, it would likely be involved in a specific function (Fig. 1a). Interestingly, it has recently been reported that the presence of the disulfide bond of *E. coli* OmpA is indispensable for the formation of the large pore [69].

Our proposed model for the role of the C-terminal domain of OmpA is summarized in Fig. 7. When the temperature is low, the vast majority of OmpA forms a two domain structure and the C-terminal domain interacts with at least the penta-peptide part of the PG-layer, which would help in holding the OM and the PG-layers together (Fig. 7a). Considering the overall shape and size of the C-terminal domain of OmpA in addition to the extended ~20 residue linker region between the two domains, the C-terminal domain can indeed reach the PG-layer that is located within 10 nm from the inner leaflet of the OM in *E. coli* [70]. Thereby OmpA, being the major outer membrane protein, would contribute to the membrane integrity of *E. coli* cell as previously reported [3] and this may be the primary function of *E. coli* OmpA. However, once the temperature is increased above the physiological temperature, the bulge structure of the C-terminal domain becomes unstable. From our results, a small fraction of it appears to form a dimer and seemingly the amount increases above physiological temperature (Fig. 4a). As mentioned above, when the structure of OmpA$^{180–325}$ is compared to the crystal structure of the C-terminal domain of *S. enterica* OmpA (Fig. 4e), the backbone r.m.s.d. is 2.0 Å. However, by excluding the bulge region (residues 281–307), the backbone r.m.s.d. is reduced to 1.4 Å, indicating that the structural differences arise mainly from the bulge region. Importantly, the bulge region is one of the interfaces for the dimerization of the C-terminal domain of *S. enterica* OmpA and helix 4 which is well defined in the structure of *E. coli* OmpA (Figs.

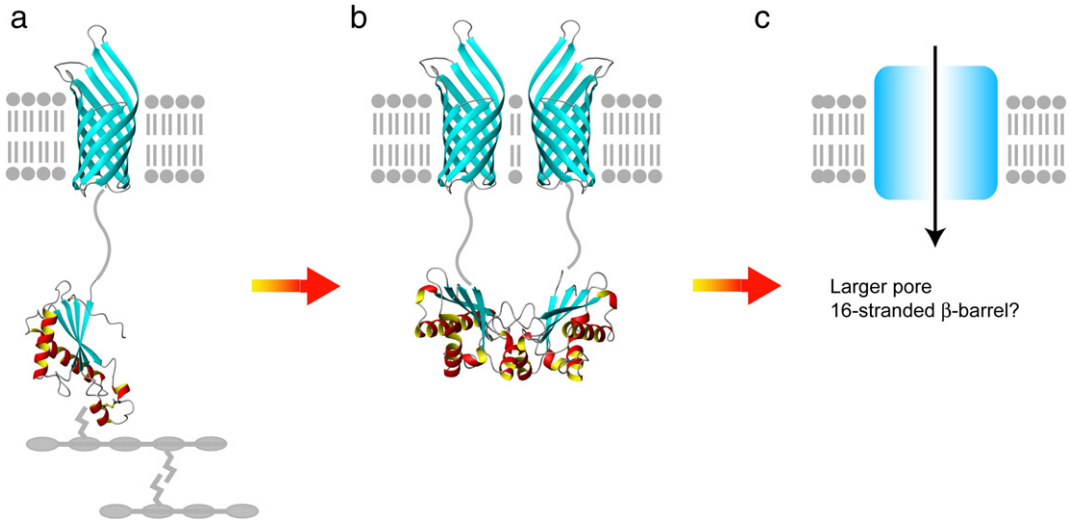

Fig. 7. A model for the role of the C-terminal domain of *E. coli* OmpA. a) At lower temperatures, the majority of OmpA forms the two domain structure; the C-terminal domain forms a highly soluble and stable globular domain and it resides in the periplasm. The flexibility and the length of the linker between the N- and C-domain enable the C-domain to reach the PG-layers and interact with the penta-peptide portion of the PG-layer. The structure of the N-terminal domain of *E. coli* OmpA was taken from the PDB (PDB ID: 1QJP). b) The destabilized bulge increases the chance of dimerization of the C-terminal domain. The crystal structure of the *Salmonella enterica* OmpA (PDB ID: 4ERH) was used to visualize the dimerization. c) The dimerized OmpA may trigger the formation of the larger pore. It seems unlikely that the large pore would be a 16 stranded β-barrel made up of two N-terminal domains, because similar 16-stranded barrels (e.g. OmpF) would have a conductance of 840 pS [75] at least twice as much as that measured for *E. coli* OmpA (~300 pS; [26]).

1b, 2 and 4e) is absent. Therefore, we suspect that a destabilized bulge structure may trigger dimerization of the C-terminal domain of *E. coli* OmpA (Fig. 7b). CD spectra of $OmpA^{180–325}$ showed decreased helical content above physiological temperature (data not shown), which is consistent with loss of structure in the bulge.

It is currently unclear how this melting behavior of the bulge region in the C-terminal domain can be directly correlated to the previously observed structural transition of *E. coli* OmpA to form the large transmembrane pore. A number of studies have suggested that the formation of the large pore also requires the conjugation of oligo-(R)-3-hydroxybutyrate groups to the C-terminal domain of OmpA. These post-translational modifications are mediated by an enzyme that is located in the periplasm [69,71]. These post-translational modifications are absent under our experimental conditions as our $OmpA^{180–325}$ protein was expressed in the cytoplasm. It is worth mentioning that the homologous OprF protein from *Pseudomonas species* has been shown to have a tendency to form an oligomer only when it forms a large pore [29]. To explain the appearance of the larger pore for *E. coli* OmpA, a model for a 16-stranded β-barrel structure that involves both the N- and C-portions of *E. coli* OmpA has been proposed [72,67]. However, such a transition would require the complete unfolding and refolding of the stable N-terminal β-barrel, as well as unfolding of the C-terminal domain, which is independently folded and also forms a stable structure. Others have already demonstrated that a properly folded OmpA C-domain can coexist with an unfolded N-domain [73]. Therefore, the possibility that more than one OmpA molecule may participate in the formation of the larger pore would necessitate the consideration of other possible structures for the large pore, perhaps being made up of two reassembled N-domains. The role of the C-domain would then be to place the two N-domains in a correct orientation and in close proximity to allow this reassembly process to occur. Alternatively, the conjugated oligo-(R)-3-hydroxybutyrate moieties on OmpA may play a direct role in the formation of the larger channel. Such compounds have indeed been shown to be able to participate directly in channel formation in *E. coli* [74]. Be that as it may, the functional significance of the large pore formation of *E. coli* OmpA in response to increasing temperatures is unknown. Perhaps, these bacteria benefit from adjusting the permeability of their outer membrane in response to changes in the temperature. Nonetheless, once formed the large pore cannot be converted back into the small pore by lowering the temperature at least not in model membrane systems [27]. Cleary, further studies including a molecular level structural characterization of the large pore are necessary for a more complete understanding of the role of the C-terminal domain of OmpA in the membrane permeability of *E. coli*.

Acknowledgements

This research was supported by operating grants from the Natural Sciences and Engineering Research Council of Canada and from the Canadian Institutes of Health Research. HJV was the holder of a Scientist award from Alberta Innovates Health Solutions.

Appendix A. Supplementary data

Supplementary data to this article can be found online at http://dx.doi.org/10.1016/j.bbamem.2014.08.008.

References

[1] W.C. Wimley, The versatile beta-barrel membrane protein, Curr. Opin. Struct. Biol. 13 (2003) 404–411.
[2] S.G. Smith, V. Mahon, M.A. Lambert, R.P. Fagan, A molecular Swiss army knife: OmpA structure, function and expression, FEMS Microbiol. Lett. 273 (2007) 1–11.
[3] I. Sonntag, H. Schwarz, Y. Hirota, U. Henning, Cell envelope and shape of *Escherichia coli*: multiple mutants missing the outer membrane lipoprotein and other major outer membrane proteins, J. Bacteriol. 136 (1978) 280–285.
[4] M. Schweizer, U. Henning, Action of a major outer cell envelope membrane protein in conjugation of *Escherichia coli* K-12, J. Bacteriol. 129 (1977) 1651–1652.
[5] W.A. Klimke, L.S. Frost, Genetic analysis of the role of the transfer gene, traN, of the F and R100-1 plasmids in mating pair stabilization during conjugation, J. Bacteriol. 180 (1998) 4036–4043.
[6] W.A. Klimke, C.D. Rypien, B. Klinger, R.A. Kennedy, J.M. Rodriguez-Maillard, L.S. Frost, The mating pair stabilization protein, TraN, of the F plasmid is an outer-membrane protein with two regions that are important for its function in conjugation, Microbiology 151 (2005) 3527–3540.
[7] S. Krishnan, N.V. Prasadarao, Outer membrane protein A and OprF: versatile roles in Gram-negative bacterial infections, FEBS J. 279 (2012) 919–931.
[8] R. Morona, M. Klose, U. Henning, *Escherichia coli* K-12 outer membrane protein (OmpA) as a bacteriophage receptor: analysis of mutant genes expressing altered proteins, J. Bacteriol. 159 (1984) 570–578.
[9] R. Koebnik, Structural and functional roles of the surface-exposed loops of the beta-barrel membrane protein OmpA from *Escherichia coli*, J. Bacteriol. 181 (1999) 3688–3694.
[10] M.L. Power, B.C. Ferrari, J. Littlefield-Wyer, D.M. Gordon, M.B. Slade, D.A. Veal, A naturally occurring novel allele of *Escherichia coli* outer membrane protein A reduces sensitivity to bacteriophage, Appl. Environ. Microbiol. 72 (2006) 7930–7932.
[11] J. Foulds, T.J. Chai, Defeat of colicin tolerance in *Escherichia coli* OmpA mutants: evidence for interaction between colicin L-JF246 and the cytoplasmic membrane, J. Bacteriol. 133 (1978) 158–164.
[12] D. Smajs, H. Pilsl, V. Braun, Colicin U, a novel colicin produced by *Shigella boydii*, J. Bacteriol. 179 (1997) 4919–4928.
[13] E. Bremer, S.T. Cole, I. Hindennach, U. Henning, E. Beck, C. Kurz, H. Schaller, Export of a protein into the outer membrane of *Escherichia coli* K12. Stable incorporation of the OmpA protein requires less than 193 amino-terminal amino-acid residues, Eur. J. Biochem. 122 (1982) 223–231.
[14] R. Chen, W. Schmidmayr, C. Krämer, U. Chen-Schmeisser, U. Henning, Primary structure of major outer membrane protein II (OmpA protein) of *Escherichia coli* K-12, Proc. Natl. Acad. Sci. U. S. A. 77 (1980) 4592–4596.
[15] G. Ried, R. Koebnik, I. Hindennach, B. Mutschler, U. Henning, Membrane topology and assembly of the outer membrane protein OmpA of *Escherichia coli* K12, Mol. Gen. Genet. 243 (1994) 127–135.
[16] H. Vogel, F. Jähnig, Models for the structure of outer-membrane proteins of *Escherichia coli* derived from raman spectroscopy and prediction methods, J. Mol. Biol. 190 (1986) 191–199.
[17] A. Pautsch, G.E. Schulz, Structure of the outer membrane protein A transmembrane domain, Nat. Struct. Biol. 5 (1998) 1013–1017.
[18] A. Pautsch, G.E. Schulz, High-resolution structure of the OmpA membrane domain, J. Mol. Biol. 298 (2000) 273–282.
[19] E. Sugawara, H. Nikaido, OmpA protein of *Escherichia coli* outer membrane occurs in open and closed channel forms, J. Biol. Chem. 269 (1994) 17981–17987.
[20] P.J. Bond, J.D. Faraldo-Gómez, M.S. Sansom, OmpA: a pore or not a pore? Simulation and modeling studies, Biophys. J. 83 (2002) 763–775.
[21] H. Hong, G. Szabo, L.K. Tamm, Electrostatic couplings in OmpA ion-channel gating suggest a mechanism for pore opening, Nat. Chem. Biol. 2 (2006) 627–635.
[22] A. Arora, F. Abildgaard, J.H. Bushweller, L.K. Tamm, Structure of outer membrane protein A transmembrane domain by NMR spectroscopy, Nat. Struct. Biol. 8 (2001) 334–338.
[23] M. Renault, O. Saurel, J. Czaplicki, P. Demange, V. Gervais, F. Löhr, V. Réat, M. Piotto, A. Milon, Solution state NMR structure and dynamics of KpOmpA, a 210 residue transmembrane domain possessing a high potential for immunological applications, J. Mol. Biol. 385 (2009) 117–130.
[24] B. Liang, A. Arora, L.K. Tamm, Fast-time scale dynamics of outer membrane protein A by extended model-free analysis of NMR relaxation data, Biochim. Biophys. Acta 1798 (2010) 68–76.
[25] H. Nikaido, Molecular basis of bacterial outer membrane permeability revisited, Microbiol. Mol. Biol. Rev. 67 (2003) 593–656.
[26] A. Arora, D. Rinehart, G. Szabo, L.K. Tamm, Refolded outer membrane protein A of *Escherichia coli* forms ion channels with two conductance states in planar lipid bilayers, J. Biol. Chem. 275 (2000) 1594–1600.
[27] E. Zakharian, R.N. Reusch, Outer membrane protein A of *Escherichia coli* forms temperature-sensitive channels in planar lipid bilayers, FEBS Lett. 555 (2003) 229–235.
[28] R. Koebnik, Proposal for a peptidoglycan-associating alpha-helical motif in the C-terminal regions of some bacterial cell-surface proteins, Mol. Microbiol. 16 (1995) 1269–1270.
[29] E. Sugawara, M. Steiert, S. Rouhani, H. Nikaido, Secondary structure of the outer membrane proteins OmpA of *Escherichia coli* and OprF of *Pseudomonas aeruginosa*, J. Bacteriol. 178 (1996) 6067–6069.
[30] E.J. Danoff, K.G. Fleming, The soluble, periplasmic domain of OmpA folds as an independent unit and displays chaperone activity by reducing the self-association propensity of the unfolded OmpA transmembrane β-barrel, Biophys. Chem. 159 (2011) 194–204.
[31] R. De Mot, J. Vanderleyden, The C-terminal sequence conservation between OmpA-related outer membrane proteins and MotB suggests a common function in both Gram-positive and Gram-negative bacteria, possibly in the interaction of these domains with peptidoglycan, Mol. Microbiol. 12 (1994) 333–334.
[32] S. Grizot, S.K. Buchanan, Structure of the OmpA-like domain of RmpM from *Neisseria meningitidis*, Mol. Microbiol. 51 (2004) 1027–1037.
[33] L.M. Parsons, F. Lin, J. Orban, Peptidoglycan recognition by Pal, an outer membrane lipoprotein, Biochemistry 45 (2006) 2122–2128.
[34] M.A. Schuler, I.G. Denisov, S.G. Sligar, Nanodiscs as a new tool to examine lipid–protein interactions, Methods Mol. Biol. 974 (2013) 415–433.
[35] T. Raschle, S. Hiller, T.Y. Yu, A.J. Rice, T. Walz, G. Wagner, Structural and functional characterization of the integral membrane protein VDAC-1 in lipid bilayer nanodiscs, J. Am. Chem. Soc. 131 (2009) 17777–17779.

[36] E. Sugawara, H. Nikaido, Pore-forming activity of OmpA protein of *Escherichia coli*, J. Biol. Chem. 267 (1992) 2507–2511.
[37] I.G. Denisov, Y.V. Grinkova, A.A. Lazarides, S.G. Sligar, Directed self-assembly of monodisperse phospholipid bilayer nanodiscs with controlled size, J. Am. Chem. Soc. 126 (2004) 3477–3487.
[38] M. Ruckert, G. Otting, Alignment of biological macromolecules in novel nonionic liquid crystalline media for NMR experiments, J. Am. Chem. Soc. 122 (2000) 7793–7797.
[39] F.A.A. Mulder, N.R. Skrynnikov, B. Hon, F.W. Dahlquist, L.E. Kay, Measurement of slow (μs–ms) time scale dynamics in protein side chains by N-15 relaxation dispersion NMR spectroscopy: application to Asn and Gln residues in a cavity mutant of T4 lysozyme, J. Am. Chem. Soc. 123 (2001) 967–975.
[40] F. Delaglio, S. Grzesiek, G.W. Vuister, G. Zhu, J. Pfeifer, A. Bax, NMRPipe: a multidimensional spectral processing system based on UNIX pipes, J. Biomol. NMR 6 (1995) 277–293.
[41] B.A. Johnson, R.A. Blevins, NMR View: a computer program for the visualization and analysis of NMR data, J. Biomol. NMR 4 (1994) 603–614.
[42] J. Jee, P. Güntert, Influence of the completeness of chemical shift assignments on NMR structures obtained with automated NOE assignment, J. Struct. Funct. Genom. 4 (2003) 179–189.
[43] Y. Shen, F. Delaglio, G. Cornilescu, A. Bax, TALOS+: a hybrid method for predicting protein backbone torsion angles from NMR chemical shifts, J. Biomol. NMR 44 (2009) 213–223.
[44] C.D. Schwieters, J.J. Kuszewski, N. Tjandra, G.M. Clore, The Xplor-NIH NMR molecular structure determination package, J. Magn. Reson. 160 (2003) 65–73.
[45] M. Zweckstetter, A. Bax, Prediction of sterically induced alignment in a dilute liquid crystalline phase: aid to protein structure determination by NMR, J. Am. Chem. Soc. 122 (2000) 3791–3792.
[46] R. Koradi, M. Billeter, K. Wuthrich, MOLMOL: a program for display and analysis of macromolecular structures, J. Mol. Graph. 14 (1996) 29–32.
[47] N. Tjandra, P. Wingfield, S. Stahl, A. Bax, Anisotropic rotational diffusion of perdeuterated HIV protease from ^{15}N NMR relaxation measurements at two magnetic fields, J. Biomol. NMR 8 (1996) 273–284.
[48] Y.M. Chook, J.V. Gray, H. Ke, W.N. Lipscomb, The monofunctional chorismate mutase from *Bacillus subtilis*. Structure determination of chorismate mutase and its complexes with a transition state analog and prephenate, and implications for the mechanism of the enzymatic reaction, J. Mol. Biol. 240 (1994) 476–500.
[49] L. Holm, C. Sander, Protein structure comparison by alignment of distance matrices, J. Mol. Biol. 233 (1993) 123–138.
[50] A. Roujeinikova, Crystal structure of the cell wall anchor domain of MotB, a stator component of the bacterial flagellar motor: implications for peptidoglycan recognition, Proc. Natl. Acad. Sci. U. S. A. 105 (2008) 10348–10353.
[51] T. Tachikawa, J. Kato, Suppression of the temperature-sensitive mutation of the bamD gene required for the assembly of outer membrane proteins by multicopy of the yiaD gene in *Escherichia coli*, Biosci. Biotechnol. Biochem. 75 (2011) 162–164.
[52] Y. Yang, D. Auguin, S. Delbecq, E. Dumas, G. Molle, V. Molle, C. Roumestand, N. Saint, Structure of the *Mycobacterium tuberculosis* OmpATb protein: a model of an oligomeric channel in the mycobacterial cell wall, Proteins 79 (2011) 645–661.
[53] C. Zheng, L. Yang, M.R. Hoopmann, J.K. Eng, X. Tang, C.R. Weisbrod, J.E. Bruce, Cross-linking measurements of in vivo protein complex topologies, Mol. Cell. Proteomics 10 (2011) (M110.006841).
[54] J. Marcoux, A. Politis, D. Rinehart, D.P. Marshall, M.I. Wallace, L.K. Tamm, C.V. Robinson, Mass spectrometry defines the C-terminal dimerization domain and enables modeling of the structure of full-length OmpA, Structure 22 (2014) 781–790.
[55] J.S. Park, W.C. Lee, K.J. Yeo, K.S. Ryu, M. Kumarasiri, D. Hesek, M. Lee, S. Mobashery, J. H. Song, S.I. Kim, J.C. Lee, C. Cheong, Y.H. Jeon, H.Y. Kim, Mechanism of anchoring of OmpA protein to the cell wall peptidoglycan of the Gram-negative bacterial outer membrane, FASEB J. 26 (2012) 219–228.
[56] K.D. Krewulak, H.J. Vogel, Structural biology of bacterial iron uptake, Biochim. Biophys. Acta 1778 (2008) 1781–1804.
[57] K.D. Krewulak, H.J. Vogel, TonB or not TonB: is that the question? Biochem. Cell Biol. 89 (2011) 87–97.
[58] T.E. Letain, K. Postle, TonB protein appears to transduce energy by shuttling between the cytoplasmic membrane and the outer membrane in *Escherichia coli*, Mol. Microbiol. 24 (1997) 271–283.
[59] P.I. Higgs, T.E. Letain, K.K. Merriam, N.S. Burke, H. Park, C. Kang, K. Postle, TonB interacts with nonreceptor proteins in the outer membrane of *Escherichia coli*, J. Bacteriol. 184 (2002) 1640–1648.
[60] N. Noinaj, M. Guillier, T.J. Barnard, S.K. Buchanan, TonB-dependent transporters: regulation, structure, and function, Annu. Rev. Microbiol. 64 (2010) 43–60.
[61] R.S. Peacock, A.M. Weljie, S.P. Howard, F.D. Price, H.J. Vogel, The solution structure of the C-terminal domain of TonB and interaction studies with TonB box peptides, J. Mol. Biol. 345 (2005) 1185–1197.
[62] E.G. Rawling, F.S. Brinkman, R.E. Hancock, Roles of the carboxy-terminal half of *Pseudomonas aeruginosa* major outer membrane protein OprF in cell shape, growth in low-osmolarity medium, and peptidoglycan association, J. Bacteriol. 180 (1998) 3556–3562.
[63] J.M. Pagès, C.E. James, M. Winterhalter, The porin and the permeating antibiotic: a selective diffusion barrier in Gram-negative bacteria, Nat. Rev. Microbiol. 6 (2008) 893–903.
[64] A.H. Delcour, Outer membrane permeability and antibiotic resistance, Biochim. Biophys. Acta 1794 (2009) 808–816.
[65] D.M. Livermore, Penicillin-binding proteins, porins and outer-membrane permeability of carbenicillin-resistant and -susceptible strains of *Pseudomonas aeruginosa*, J. Med. Microbiol. 18 (1984) 261–270.
[66] R. Koebnik, K.P. Locher, P. Van Gelder, Structure and function of bacterial outer membrane proteins: barrels in a nutshell, Mol. Microbiol. 37 (2000) 239–253.
[67] R.N. Reusch, Insights into the structure and assembly of *Escherichia coli* outer membrane protein A, FEBS J. 279 (2012) 894–909.
[68] P.A. Manning, A.P. Pugsley, P. Reeves, Defective growth functions in mutants of *Escherichia coli* K12 lacking a major outer membrane protein, J. Mol. Biol. 116 (1977) 285–300.
[69] A. Negoda, E. Negoda, R.N. Reusch, Resolving the native conformation of *Escherichia coli* OmpA, FEBS J. 277 (2010) 4427–4437.
[70] W. Vollmer, S.J. Seligman, Architecture of peptidoglycan: more data and more models, Trends Microbiol. 18 (2010) 59–66.
[71] R.N. Reusch, The role of short-chain conjugated poly-(R)-3-hydroxybutyrate (cPHB) in protein folding, Int. J. Mol. Sci. 14 (2013) 10727–10748.
[72] C. Stathopoulos, An alternative topological model for *Escherichia coli* OmpA, Protein Sci. 5 (1996) 170–173.
[73] T.A. Walton, C.M. Sandoval, C.A. Fowler, A. Pardi, M.C. Sousa, The cavity-chaperone Skp protects its substrate from aggregation but allows independent folding of substrate domains, Proc. Natl. Acad. Sci. U. S. A. 106 (2009) 1772–1777.
[74] E. Pavlov, C. Grimbly, C.T. Diao, R.J. French, A high-conductance mode of a poly-3-hydroxybutyrate/calcium/polyphosphate channel isolated from competent *Escherichia coli* cells, FEBS Lett. 579 (2005) 5187–5192.
[75] P.S. Phale, T. Schirmer, A. Prilipov, K.L. Lou, A. Hardmeyer, J.P. Rosenbusch, Voltage gating of *Escherichia coli* porin channels: role of the constriction loop, Proc. Natl. Acad. Sci. U. S. A. 94 (1997) 6741–6745.